

# The pairwise velocity probability density function in models with local primordial non-Gaussianity

Tsz Yan Lam<sup>1\*</sup>, Takahiro Nishimichi<sup>1\*</sup> & Naoki Yoshida<sup>1\*</sup>

<sup>1</sup> *Institute for the Physics and Mathematics of the Universe, University of Tokyo, Kashiwa, Chiba 277-8583, Japan*

15 February 2022

## ABSTRACT

We study how primordial non-Gaussianity affects the pairwise velocity probability density function (PDF) using an analytical model and cosmological  $N$ -body simulations. We adopt the local type non-Gaussian models characterized by  $f_{nl}$ , and examine both the linear velocity difference PDF and the linear pairwise velocity PDF. We show explicitly how  $f_{nl}$  induces correlations between originally independent velocities along the parallel and the perpendicular to the line of separation directions. We compare the model results with measurements from  $N$ -body simulations of the non-Gaussian models. Linear theory fails to predict the PDF in the  $f_{nl}$  models. Therefore we develop an analytic model based on the Zeldovich approximation to describe the evolution of the velocity PDF. Our analytical model and simulation results show remarkably good agreement in both the parallel and the perpendicular directions for the PDF profiles, as well as the change in the PDF due to primordial non-Gaussianity. The agreement is particularly good for relatively small separations ( $< 10h^{-1}\text{Mpc}$ ). The inclusion of the evolution of the velocity PDF is important to obtain a good description on the signature of primordial non-Gaussianity in the PDF. Our model provides the foundation to constrain  $f_{nl}$  using the peculiar velocity in future surveys.

**Key words:** methods: analytical - dark matter - large scale structure of the universe

## 1 INTRODUCTION

Primordial non-Gaussianity has attracted much attention owing to its ability to distinguish inflationary models (e.g., Buchbinder et al. 2008; Khoury & Piazza 2008; Silvestri & Trodden 2008; Wands 2010, and references therein). Several cosmological probes using the CMB (Komatsu et al. 2010; Hikage et al. 2008; Yadav & Wandelt 2008; McEwen et al. 2008; Rossi et al. 2009; Smidt et al. 2010; Komatsu 2010; Rossi et al. 2010) and the large-scale structures in the Universe (Koyama et al. 1999; Matarrese et al. 2000; Scoccimarro et al. 2004; Sefusatti & Komatsu 2007; Izumi & Soda 2007; Lo Verde et al. 2008; Dalal et al. 2008; Matarrese & Verde 2008; Carbone et al. 2008; Afshordi & Tolley 2008; Slosar et al. 2008; McDonald 2008; Taruya et al. 2008; Slosar 2009; Grossi et al. 2008; Kamionkowski et al. 2009; Desjacques et al. 2009; Pillepich et al. 2008; Lam & Sheth 2009; Grossi et al. 2009; Lam et al. 2009, 2010; Nishimichi et al. 2009; Cunha et al. 2010; Sartoris et al. 2010; Desjacques & Seljak 2010a; Liguori et al. 2010; Tseliakhovich et al. 2010; Xia et al. 2010; Chongchitnan & Silk 2010; Giannantonio & Porciani 2010; Marian et al. 2010; Smith et al. 2010) have been considered.

Here, we introduce a new large-scale structure probe of primordial non-Gaussianity – the pairwise velocity PDF. Current large-scale structure probes of primordial non-Gaussianity focus on the clustering of halos, halo/void abundances, bispectrum, and the PDF of dark matter field – all of them are related to the change of the density field due to primordial non-Gaussianity. It is important to note that both the initial density field and the initial velocity field are generated from the primordial perturbation, and that their linear relation is described by the continuity equation. Hence, one may naively expect that primordial non-Gaussianity affect the velocity field as well as the density field. While various measurements associated with the change of density field have been extensively studied, there are few studies on the effect of primordial non-Gaussianity on the velocity field. Scherrer (1992); Catelan & Scherrer (1995) discussed the effect of primordial non-Gaussianity on the

\* E-mail: tszyan.lam@ipmu.jp

distributions of linear velocity fields. In particular Catelan & Scherrer (1995) studied the distribution of the parallel component of the pairwise velocity using linear theory. Lam et al. (2010) discussed the effect of primordial non-Gaussianity on the redshift space distortion. They made use of the ellipsoidal collapse model to derive the modification in the Kaiser factor relating the real and redshift space power spectra, without discussing the modification in the velocity field. During the preparation of this work, Schmidt (2010) studied the primordial non-Gaussianity signature in the peculiar velocities of density peaks using linear theory. Our present study has two important improvements over these previous works: first we show that primordial non-Gaussianity induces a correlation between velocities in the parallel and the perpendicular to the line of separation directions. We show explicitly how this correlation, which is absent in Schmidt (2010), modifies significantly the linear velocity PDF. Secondly, we show that the linear theory does not provide a good description of the signature of  $f_{nl}$  in the pairwise velocity PDF even at separation as big as  $50 h^{-1}\text{Mpc}$ . We use cosmological  $N$ -body simulations to show this. We thus develop an analytic model to describe the evolution of the velocity PDF. Our model is based on the Zeldovich Approximation. We illustrate the improvement in the  $N$ -body measurement comparisons.

The peculiar velocity field has been investigated as a probe of cosmology for both dark matter (Gorski 1988; Seto & Yokoyama 1998; Sheth et al. 2001; Kuwabara et al. 2002; Scoccimarro 2004) and biased tracers (Sheth & Diaferio 2001; Sheth et al. 2001; Hamana et al. 2003; Sheth & Zehavi 2009). Other studies (Yoshida et al. 2001; Peel 2006; Bhattacharya & Kosowsky 2007, 2008) discuss the possibility of constraining dark energy via the kinetic Sunyaev-Zeldovich effect. In this study we focus on the peculiar velocity field of the dark matter field. The effect of primordial non-Gaussianity on the velocity of biased tracers will be discussed in future work.

We first describe how the linear velocity PDF changes due to primordial non-Gaussianity in section 2. Throughout the present paper, we work with models with non-vanishing primordial bispectrum; we will use the local  $f_{nl}$  type primordial non-Gaussianity to illustrate the calculations. The Bardeen potential  $\Phi$  in the local  $f_{nl}$  model is

$$\Phi = \phi + f_{nl}(\phi^2 - \langle \phi^2 \rangle), \quad (1)$$

where  $\phi$  is a Gaussian potential field and  $f_{nl}$  is the nonlinear quadratic parameter. The above non-Gaussian correction is defined at  $z = z_{CMB}$  for this study. It has been suggested that mass weighting is important for the peculiar velocities (Scoccimarro 2004; Sheth & Zehavi 2009). We will discuss the effect of primordial non-Gaussianity on both the uniform weighted as well as the mass weighted linear velocity PDF. In section 3 we describe the analytical model to approximate the evolution of the pairwise velocity PDF. The theoretical predictions of both the linear theory and the analytical model are compared with measurements from  $N$ -body simulations. We conclude our findings in section 4.

## 2 LINEAR VELOCITY PDF

### 2.1 Preliminary

The linear overdensity  $\delta(k)$  and the Bardeen potential  $\Phi(k)$  is related by the Poisson equation

$$\delta(k, z) = D(z)k^2 M(k)\Phi(k), \quad (2)$$

where  $M(k) = 2c^2 T(k)/3\Omega_m H_0^2$  and  $T(k)$  is the matter transfer function (note we do not include the  $k^2$  factor in  $M(k)$ ). The continuity relates the linear overdensity and the peculiar velocity  $\mathbf{u}(\mathbf{k}, z)$ :

$$\dot{\delta}(\mathbf{k}) + \theta(\mathbf{k}) = 0, \quad (3)$$

where  $\theta(\mathbf{x}) \equiv \nabla \cdot \mathbf{u}(\mathbf{x})$  is the divergence of the velocity field. The velocity field is described solely by its divergence since its vorticity decays due to the expansion of the universe (for example see Bernardeau et al. 2002). Hence

$$u_j(k) = i\dot{D}(z)k_j M(k)\Phi(k), \quad (4)$$

where  $i^2 = -1$  and the subscript  $j$  denotes the coordinate of the peculiar velocity. In this study we will be interested in the relative velocities in the parallel ( $\parallel$ ) and perpendicular ( $\perp_a$  and  $\perp_b$ ) to the line of separation for two particles separated by some distance  $r$ .

Connected moments higher than the second order vanish when the Bardeen potential is Gaussian. When the primordial perturbation is non-Gaussian, the leading order of the non-vanishing connected moment (higher than the second order) depends on the particular model of primordial non-Gaussianity. Most studies in the literature concern with models with a non-vanishing bispectrum (including the local  $f_{nl}$  and the equilateral triangle type  $f_{nl}$ ). Some other studies investigate models with a non-vanishing trispectrum (the  $g_{nl}$  model, see for example Desjacques & Seljak 2010b). While this work focuses on primordial non-Gaussianity with a leadingly non-vanishing bispectrum, it can be extended to study models where the leading order of the non-vanishing connected moment is higher than the third order. In what follows we will use the local  $f_{nl}$  model to demonstrate how the non-vanishing third order connected moment modifies the pairwise velocity PDF. The calculation can also apply to models with other types of primordial bispectrum.

We denote the peculiar velocity at position  $\mathbf{x}$  by  $\mathbf{u}(\mathbf{x})$  and the relative velocity by  $\mathbf{v}(\mathbf{r}) \equiv \mathbf{u}(\mathbf{x}) - \mathbf{u}(\mathbf{x}') = \mathbf{u} - \mathbf{u}'$  where

$\mathbf{x} - \mathbf{x}' = \mathbf{r}$ . We also denote the velocity difference PDF  $p(\mathbf{v}; r)$  as the PDF of the peculiar velocity difference at two random positions separated by  $r$ ; the pairwise velocity PDF  $q(\mathbf{v}; r)$  as the PDF of the difference of the peculiar velocities of two tested particles separated by  $r$ . The latter PDF is the pair weighted version of the former one and they are in general not equivalent (see, for example Scoccimarro 2004). For simplicity we sometimes call the former PDF the uniform weighted PDF and the latter one the mass/pair weighted PDF.

The numerical integration of the third order connected moments are carried out by Monte-Carlo integration using the numerical package *CUBA* (Hahn 2005).

## 2.2 Linear Velocity Difference PDF

### 2.2.1 Case: $f_{nl} = 0$

The linear velocity difference PDF of two random positions separated by a distance  $r$  when  $f_{nl} = 0$  is given by the multivariate normal distribution:

$$p_0(\mathbf{v}; r) = \frac{1}{(2\pi)^{3/2} \sqrt{|A|}} \exp\left(-\frac{1}{2} \mathbf{v}^T A^{-1} \mathbf{v}\right), \quad (5)$$

where  $\mathbf{v} = (v_{\parallel}, v_{\perp a}, v_{\perp b})$  in which  $v_{\parallel}$  corresponds to the relative velocity parallel to the line of separation and  $v_{\perp a}$  and  $v_{\perp b}$  are the two velocity differences perpendicular to the line of separation. Here  $A$  is the covariance matrix. The above expression simplifies since there is no correlation between different components of  $\mathbf{v}$ . Hence the r.h.s becomes a product of three univariate normal distributions:

$$p_0(v_{\parallel}, v_{\perp a}, v_{\perp b}; r) = p_0(v_{\parallel}; r) p_0(v_{\perp a}; r) p_0(v_{\perp b}; r), \quad (6)$$

where the variances of the univariate normal distributions are  $\langle v_{\parallel}^2 \rangle$  and  $\langle \mathbf{v}_{\perp}^2 \rangle \equiv \langle v_{\perp a}^2 \rangle = \langle v_{\perp b}^2 \rangle$  respectively, and

$$\langle v_{\parallel}^2 \rangle = \frac{1}{3\pi^2} \dot{D}_0^2 \int dk P_{\Phi}(k) k^4 M^2(k) \left[ 1 - 3j_0(kr) + 6\frac{j_1(kr)}{kr} \right] \quad (7)$$

$$\langle \mathbf{v}_{\perp}^2 \rangle = \frac{1}{3\pi^2} \dot{D}_0^2 \int dk P_{\Phi}(k) k^4 M^2(k) \left[ 1 - 3\frac{j_1(kr)}{kr} \right]. \quad (8)$$

Here  $j_0$  and  $j_1$  is the spherical bessel function,  $\dot{D}_0 = dD/dt$  is the time derivative of the linear growth factor  $D$  at  $z = 0$  and  $P_{\Phi}(k) \approx P_{\phi}(k)$  is the Bardeen potential power spectrum. Iostropy means one can transform the rectangular coordinate in the plane perpendicular to the line of separation into the polar coordinate and write equation (6) as

$$p_0(v_{\parallel}, v_{\perp a}, v_{\perp b}; r) dv_{\parallel} dv_{\perp a} dv_{\perp b} = 2\pi v_{\perp} p_0(v_{\parallel}; r) p_0(v_{\perp}; r) dv_{\parallel} dv_{\perp}, \quad (9)$$

where  $v_{\perp}^2 = v_{\perp a}^2 + v_{\perp b}^2$ . Notice that our notations  $\langle \mathbf{v}_{\perp} \cdots \rangle (= \langle v_{\perp a} \cdots \rangle = \langle v_{\perp b} \cdots \rangle)$  and  $v_{\perp} (= \sqrt{v_{\perp a}^2 + v_{\perp b}^2})$  are not equivalent.

### 2.2.2 Case: $f_{nl} \neq 0$

When  $f_{nl} \neq 0$ , the primordial bispectrum is non-zero and its functional form in the local type is

$$B_{\Phi}(k_1, k_2, k_{12}) = 2f_{nl}[P(k_1)P(k_2) + \text{cyclic}] + \mathcal{O}(f_{nl}^3). \quad (10)$$

Connected moments higher than the second order are non-vanishing and contribute to the velocity difference PDF. The leadingly non-vanishing connected moments are

$$\begin{aligned} \frac{\langle v_{\parallel}^3 \rangle}{2f_{nl}} &= \frac{12\dot{D}_0^3}{(2\pi)^6} \int d^3 \mathbf{k}_1 \int_{\cos \mu_2 \geq 0} d^3 \mathbf{k}_2 P(k_1) P(k_2) M(k_1) M(k_2) M(k_{12}) k_{1\parallel} k_{2\parallel} k_{12\parallel} [\sin(k_{12\parallel} r) - 2\sin(k_{2\parallel} r)] \\ \frac{\langle v_{\parallel} v_{\perp a}^2 \rangle}{2f_{nl}} &\equiv \frac{\langle v_{\parallel} v_{\perp a}^2 \rangle}{2f_{nl}} = \frac{\langle v_{\parallel} v_{\perp b}^2 \rangle}{2f_{nl}} = \frac{4\dot{D}_0^3}{(2\pi)^6} \int d^3 \mathbf{k}_1 \int_{\cos \mu_2 \geq 0} d^3 \mathbf{k}_2 P(k_1) P(k_2) M(k_1) M(k_2) M(k_{12}) [k_{1\perp} k_{2\perp} k_{12\parallel} \sin(k_{12\parallel} r) \\ &\quad - 2k_{1\perp} k_{2\parallel} k_{12\perp} \sin(k_{2\parallel} r) + 2k_{1\perp} k_{2\parallel} k_{12\perp} \sin(k_{12\parallel} r) - 2k_{1\parallel} k_{2\perp} k_{12\perp} \sin(k_{2\parallel} r) - 2k_{1\perp} k_{2\perp} k_{12\parallel} \sin(k_{2\parallel} r)], \end{aligned} \quad (11)$$

where  $k_{12} = |k_1 + k_2|$ ,  $k_{i\parallel} = k_i \cos \mu_i$ ,  $k_{i\perp} = k_i \sin \mu_i \cos \phi_i$ , and  $k_{12\parallel} = k_{1\parallel} + k_{2\parallel}$  (similarly for  $\perp$ ). Note that connected moments involving odd power of  $v_{\perp}$  vanish irrespective of the value of  $f_{nl}$ . The non-vanishing component  $\langle v_{\parallel} v_{\perp}^2 \rangle$  results in couplings between velocities in the parallel and the perpendicular to the line of separation directions. As a result the linear multivariate PDF can no longer be written as a product of three independent univariate PDFs. We use the tri-variate Edgeworth expansion to approximate the linear uniform weighted velocity difference PDF for  $f_{nl} \neq 0$  (see appendix for derivation):

$$p(v_{\parallel}, v_{\perp a}, v_{\perp b}; f_{nl}, r) = p_0(v_{\parallel}, v_{\perp a}, v_{\perp b}; r) [1 + \alpha_{300} h_{300} + \alpha_{120} (h_{120} + h_{102})], \quad (13)$$

where

$$\alpha_{300} = \frac{1}{6} \frac{\langle v_{\parallel}^3 \rangle}{\langle v_{\parallel}^2 \rangle^{3/2}}, \quad \alpha_{120} = \frac{1}{2} \frac{\langle v_{\parallel} v_{\perp}^2 \rangle}{\langle v_{\parallel}^2 \rangle^{1/2} \langle \mathbf{v}_{\perp}^2 \rangle},$$

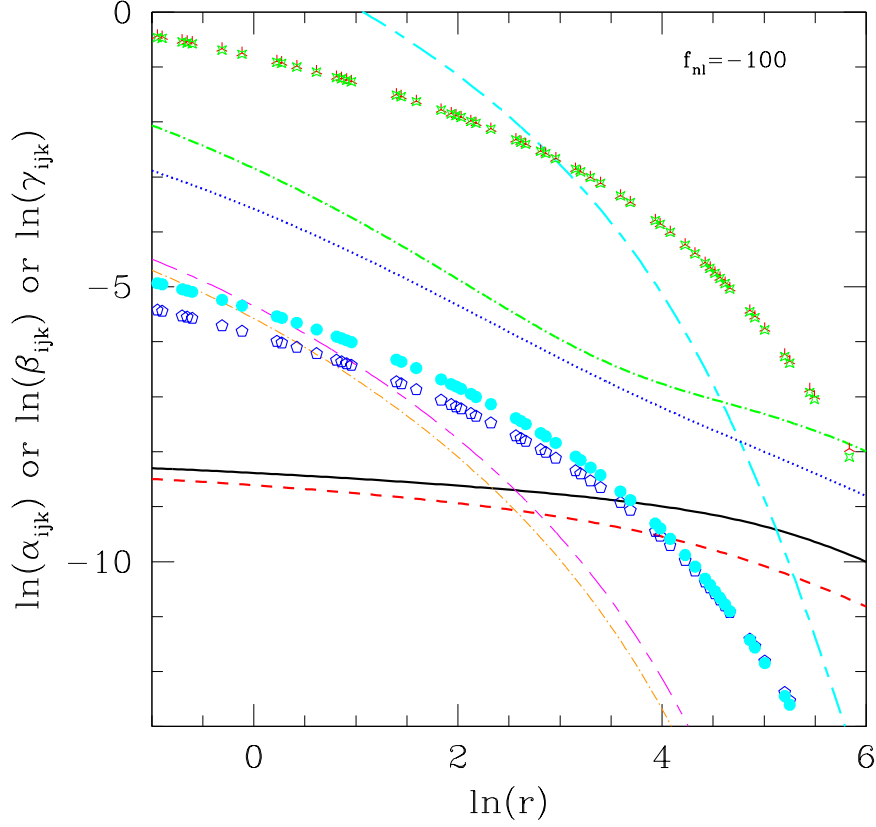


**Figure 1.** Scale dependence of parameters:  $\alpha_{300}$  (thick solid black curve),  $\alpha_{120}$  (thick dashed red curve),  $-\beta_{100}$  (red skeletal triangular symbols),  $\beta_{200}$  (thick cyan short-long-dashed curve),  $-\gamma_{100}$  (green starred symbols),  $\gamma_{300}$  (thick green dot-dashed curve),  $\gamma_{120}$  (thick blue dotted curve),  $-\gamma_{400}$  (blue pentagons),  $-\gamma_{220}$  (cyan hexagons),  $\gamma_{500}$  (thin magenta short-long-dashed curve), and  $\gamma_{320}$  (thin orange dot-dashed curve).  $f_{nl} = -100$  for those parameters apply.  $\alpha_{300}$ ,  $\alpha_{120}$ ,  $-\gamma_{100}$ , and  $-\beta_{100}$  are shifted vertically by -2 for clarity.

and  $h_{ijk} \equiv H_i(\nu_{\parallel})H_j(\nu_{\perp a})H_k(\nu_{\perp b})$  is the product of Hermite polynomials of different orders. In particular,

$$h_{300} \equiv \nu_{\parallel}^3 - 3\nu_{\parallel} = \frac{v_{\parallel}^3}{\langle v_{\parallel}^2 \rangle^{3/2}} - 3 \frac{v_{\parallel}}{\langle v_{\parallel}^2 \rangle^{1/2}} \quad (14)$$

$$h_{120} \equiv \nu_{\parallel}(\nu_{\perp a}^2 - 1) = \frac{v_{\parallel}}{\langle v_{\parallel}^2 \rangle^{1/2}} \left( \frac{v_{\perp a}^2}{\langle v_{\perp}^2 \rangle} - 1 \right) \quad (15)$$

$$h_{102} \equiv \nu_{\parallel}(\nu_{\perp b}^2 - 1) = \frac{v_{\parallel}}{\langle v_{\parallel}^2 \rangle^{1/2}} \left( \frac{v_{\perp b}^2}{\langle v_{\perp}^2 \rangle} - 1 \right). \quad (16)$$

Note that Schmidt (2010) marginalized velocities perpendicular to the line of separation, essentially setting  $\alpha_{120} = 0$ .

Figure 1 shows the scale dependence of  $\alpha_{300}$  (thick solid black curve) and  $\alpha_{120}$  (thick dashed red curve) for  $f_{nl} = -100$ . While the numerical value is small compared to unity, the effect of non-zero  $f_{nl}$  becomes significant for big  $|\nu_{\parallel}|$  or  $|\nu_{\perp}|$ . Furthermore  $\alpha_{300}$  and  $\alpha_{120}$  are in the same order of magnitude, hence both terms have to be included in the computation of the linear peculiar velocity difference PDF.

Figure 2 shows the ratios of the linear peculiar velocity difference PDF for  $f_{nl} = 100$  to the corresponding Gaussian PDF at  $r = 8 h^{-1}\text{Mpc}$ . The axes labeled  $v_{\parallel}$  indicates the velocity in the parallel to the line of separation direction and  $v_{\perp}$  is the magnitude of the velocity perpendicular to the line of separation (recall  $v_{\perp} = \sqrt{v_{\perp a}^2 + v_{\perp b}^2}$ ). The upper panel shows both the contour and color maps over a wide range of velocity. The effect of primordial non-Gaussianity is most significant at extreme velocities. Both the contour and the color maps show variations in the ratio for different values of  $v_{\perp}$  at fixed  $v_{\parallel}$ , indicating that the modification due to  $f_{nl}$  is degenerated in the plane of  $(v_{\parallel}, v_{\perp})$ . While the upper panel shows that the ratio can be as big as 4, the first order Edgeworth expansion breaks down in such rare cases (about  $10\text{-}\sigma$  level) – it is evident by the negative probability at the other end of the plot.

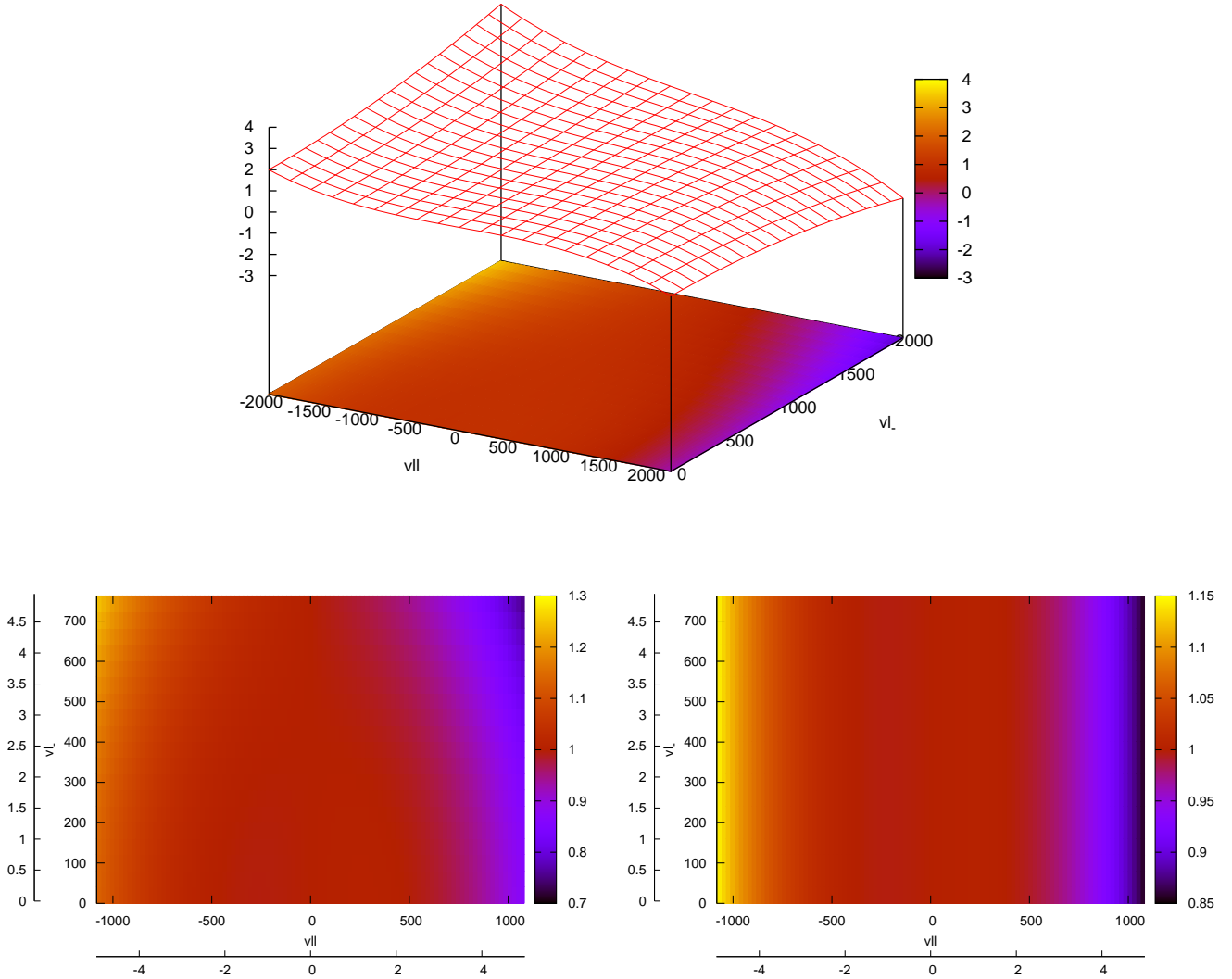


**Figure 2.** Ratio of linear velocity difference PDF  $p/p_0$  in equation (13) for  $r = 8 h^{-1}\text{Mpc}$  and  $f_{nl} = 100$ .  $v_{||}$  indicates velocity in the parallel to the line of separation direction while  $v_{\perp}$  is the magnitude of the velocity perpendicular to the line of separation. Upper panel shows the ratio for a wide range of velocity. The lower left panel zooms into regions for around  $5\text{-}\sigma$  as indicated by the outer axes. The lower right panel shows the same regions as the lower left panel, but explicitly set the parameter  $\alpha_{120} = 0$  as previous study did.

The lower panels of Figure 2 show the color maps of the same PDF ratio on a smaller velocity range to increase the dynamic range of the effect of  $f_{nl}$  on the linear velocity difference PDF. The left panel shows the modification obtained in this study (the correction term in equation (13)) while the right panel shows the result for setting  $\langle v_{||}v_{\perp}^2 \rangle = 0$ . The outer axes of the lower panels show the  $\sigma$ -level in corresponding directions. At  $5\text{-}\sigma$  level ( $v_{||}$  direction) the change is about 30%, and the bigger the  $\sigma$ -level in the perpendicular direction the greater the modification is. The linear theory suggests that for  $f_{nl} > 0$  the infalling probability (negative velocity) is enhanced while the outgoing probability (positive velocity) is decreased. This trend applies to other scales we looked at (from 4 to  $100 h^{-1}\text{Mpc}$ ). While it is generally believed that linear theory applies for large scales, we will show in the next section that linear theory fails to describe the change in the velocity PDF due to  $f_{nl}$  even at separation as big as  $50 h^{-1}\text{Mpc}$ .

### 2.3 Linear Pairwise Velocity PDF

It is widely accepted that, while the linear theory prediction is a good approximation for large scales ( $\gtrsim 20 h^{-1}\text{Mpc}$ ), the linear theory velocity correlations of massive halos (in the parallel to the line of separation direction) is not consistent with

$N$ -body measurements (Croft & Efstathiou 1995). Sheth & Zehavi (2009) pointed out that the velocity correlations of biased tracers, in both parallel and perpendicular to the line of separation directions, can in fact be reasonably described by linear theory when proper pair-weighting is included. While our current study focuses on the difference of the peculiar velocities of unbiased tracer, it is useful to examine whether the pair weighting would improve the linear theory prediction. It is reasonable to include this mass weighting as the pairwise velocity PDF measured in  $N$ -body simulations is obtained by counting the relative velocities of simulated particles. As a result regions with more particles (overdense regions) have a bigger weight than regions with less particles (underdense regions).

### 2.3.1 Case: $f_{nl} = 0$

Scoccimarro (2004) discussed how to generalize the linear velocity difference PDF when  $f_{nl} = 0$  to include the mass weighting. The resulting linear pairwise velocity PDF  $q_0$  is related to the associated no weighting velocity difference PDF  $p_0$  by

$$[1 + \xi(r)] \frac{q_0(\nu_{\parallel}, \nu_{\perp a}, \nu_{\perp b}; r)}{p_0(\nu_{\parallel}, \nu_{\perp a}, \nu_{\perp b}; r)} = 1 + \xi(r) + h_{100}\beta_{100} + h_{200}\beta_{200}, \quad (17)$$

where  $\delta \equiv \delta(\mathbf{x})$ ,  $\delta' \equiv \delta(\mathbf{x} + r)$ ,  $\xi \equiv \xi(r) = \langle \delta \delta' \rangle$  is the matter correlation function at separation  $r$ , and

$$\beta_{100} = \frac{\langle v_{\parallel} \delta \rangle}{\langle v_{\parallel}^2 \rangle^{1/2}} + \frac{\langle v_{\parallel} \delta' \rangle}{\langle v_{\parallel}^2 \rangle^{1/2}}, \quad \beta_{200} = \frac{\langle v_{\parallel} \delta \rangle \langle v_{\parallel} \delta' \rangle}{\langle v_{\parallel}^2 \rangle}, \quad (18)$$

$$\langle v_{\parallel} \delta \rangle = \langle v_{\parallel} \delta' \rangle = \frac{1}{2\pi^2} \dot{D}_0 \int dk P_{\Phi}(k) k^4 M^2(k) [k j_1(kr)]. \quad (19)$$

The r.h.s of equation (17) does not depend  $v_{\perp}$ , hence  $q_0$  can still be written as a product of three univariate PDFs – the correction term on the r.h.s of equation (17) only modifies the univariate PDF of  $v_{\parallel}$ . The scale dependence of the parameters  $-\beta_{100}$  (red sketeal triangular symbols) and  $\beta_{200}$  (thick cyan short-long-dashed curve) are shown in Figure 1: their magnitudes are big compared to others shown in the same figure since they are 'Gaussian parameters' that do not depend on  $f_{nl}$ .

### 2.3.2 Case: $f_{nl} \neq 0$

When  $f_{nl} \neq 0$  additional terms contribute to the mass weighted linear velocity difference PDF. To the first order of  $f_{nl}$  the expression is (see derivation in appendix)

$$[1 + \xi(r)] \frac{q(\nu_{\parallel}, \nu_{\perp a}, \nu_{\perp b}; f_{nl}, r)}{p_0(\nu_{\parallel}, \nu_{\perp a}, \nu_{\perp b}; r)} = 1 + \xi(r) + h_{100}\gamma_{100} + h_{200}\beta_{200} + h_{300}\gamma_{300} + (h_{120} + h_{102})\gamma_{120} \\ + h_{400}\gamma_{400} + (h_{220} + h_{202})\gamma_{220} + h_{500}\gamma_{500} + (h_{320} + h_{302})\gamma_{320}, \quad (20)$$

where

$$\begin{aligned} \gamma_{100} &= \beta_{100} + \frac{\langle v_{\parallel} \delta \delta' \rangle}{\langle v_{\parallel}^2 \rangle^{1/2}} & \gamma_{300} &= \alpha_{300}(1 + \xi(r)) + \frac{\beta_{100}}{2} \frac{\langle v_{\parallel}^2 \delta' \rangle}{\langle v_{\parallel}^2 \rangle} & \gamma_{120} &= \alpha_{120}(1 + \xi(r)) + \frac{\beta_{100}}{2} \frac{\langle \mathbf{v}_{\perp}^2 \delta' \rangle}{\langle \mathbf{v}_{\perp}^2 \rangle} \\ \gamma_{400} &= \alpha_{300} \frac{\beta_{100}}{2} & \gamma_{220} &= \alpha_{120} \beta_{100} & \gamma_{500} &= \alpha_{300} \beta_{200} \\ \gamma_{320} &= \alpha_{120} \beta_{200} & h_{400} &= \nu_{\parallel}^4 - 6\nu_{\parallel}^2 + 3 & h_{500} &= \nu_{\parallel}^5 - 10\nu_{\parallel}^3 + 15\nu_{\parallel}, \end{aligned}$$

and for the local  $f_{nl}$  type primordial non-Gaussianity

$$\frac{\langle v_{\parallel} \delta \delta' \rangle}{2f_{nl}} = -\frac{4\dot{D}_0}{(2\pi)^6} \int d^3 \mathbf{k}_1 \int_{\cos \mu_2 \geq 0} d^3 \mathbf{k}_2 P(k_1) P(k_2) M(k_1) M(k_2) M(k_{12}) [k_{1\parallel} k_2^2 k_{12}^2 \sin(k_{12\parallel} r) + k_1^2 k_2^2 k_{12\parallel} \sin(k_{2\parallel} r) \\ - k_{1\parallel} k_2^2 k_{12}^2 \sin(k_{2\parallel} r)] \quad (21)$$

$$\frac{\langle v_{\parallel}^2 \delta' \rangle}{2f_{nl}} = \frac{2\dot{D}_0^2}{(2\pi)^6} \int d^3 \mathbf{k}_1 \int_{\cos \mu_2 \geq 0} d^3 \mathbf{k}_2 P(k_1) P(k_2) M(k_1) M(k_2) M(k_{12}) [2k_{1\parallel} k_2^2 k_{12\parallel} \cos(k_{2\parallel} r) - k_{1\parallel} k_{2\parallel} k_{12}^2 \cos(k_{12\parallel} r) \\ + 2k_{1\parallel} k_{2\parallel} k_{12}^2 \cos(k_{2\parallel} r) - 2k_{1\parallel} k_2^2 k_{12\parallel} \cos(k_{1\parallel} r) - 2k_{1\parallel} k_2^2 k_{12\parallel} \cos(k_{12\parallel} r) + 2k_{1\parallel} k_2^2 k_{12\parallel} - k_{1\parallel} k_{2\parallel} k_{12}^2] \quad (22)$$

$$\frac{\langle \mathbf{v}_{\perp}^2 \delta' \rangle}{2f_{nl}} = \frac{2\dot{D}_0^2}{(2\pi)^6} \int d^3 \mathbf{k}_1 \int_{\cos \mu_2 \geq 0} d^3 \mathbf{k}_2 P(k_1) P(k_2) M(k_1) M(k_2) M(k_{12}) [2k_{1\perp} k_2^2 k_{12\perp} \cos(k_{2\parallel} r) - k_{1\perp} k_{2\perp} k_{12}^2 \cos(k_{12\parallel} r) \\ + 2k_{1\perp} k_{2\perp} k_{12}^2 \cos(k_{2\parallel} r) - 2k_{1\perp} k_2^2 k_{12\perp} \cos(k_{1\parallel} r) - 2k_{1\perp} k_2^2 k_{12\perp} \cos(k_{12\parallel} r) + 2k_{1\perp} k_2^2 k_{12\perp} - k_{1\perp} k_{2\perp} k_{12}^2]. \quad (23)$$

The scale dependences of  $\gamma_{ijk}$  are shown in figure 1. As in the case of uniform weighted linear PDF, the linear pairwise velocity PDF can no longer be written as a product of three independent PDFs when  $f_{nl} \neq 0$  due to the non-vanishing terms  $\langle v_{\parallel} \mathbf{v}_{\perp}^2 \rangle$  and  $\langle \mathbf{v}_{\perp}^2 \delta' \rangle$ . In addition, when one sets  $\delta = \delta' = 0$ , the above expression recovers the uniform weighted linear PDF for  $f_{nl} \neq 0$  (equation (13)).

Figure 3 shows the modification factor of the linear pairwise velocity PDF due to  $f_{nl}$  ( $q/q_0$  in equations (17) and (20)). As

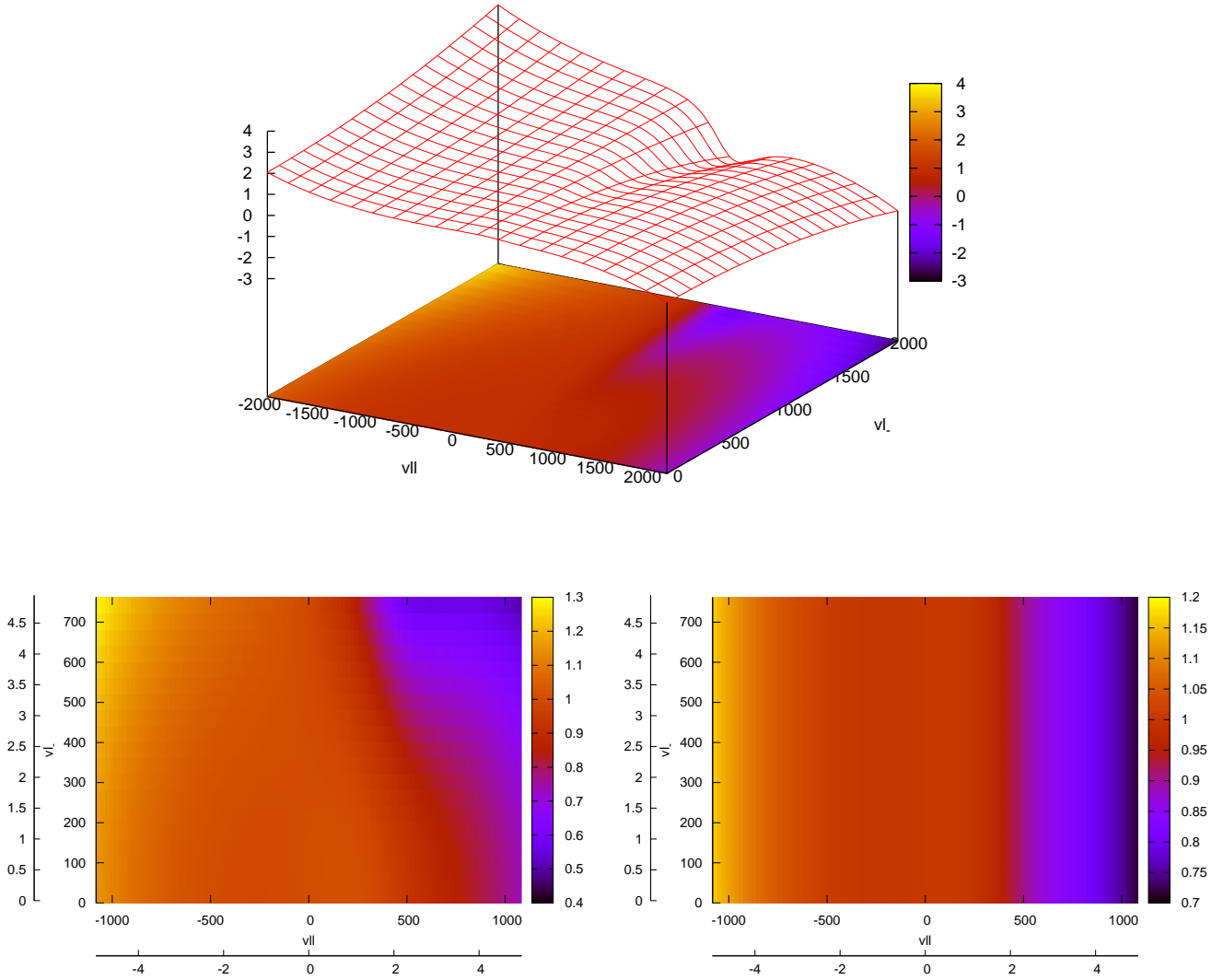


**Figure 3.** Similar plot to figure 2 but for the ratio of the linear pairwise velocity PDF ( $q/q_0$  in equations (17) and (20)). The lower right panel sets  $\alpha_{120} = \gamma_{220} = \gamma_{320} = \langle v_{\perp}^2 \delta' \rangle = 0$ .

in Figure 2 the upper panel shows the ratio in a wide range of velocity, including regions with negative probability indicating the breakdown of the first order Edgeworth expansion approximation. The lower left panel enlarges the color map on regions about  $5\text{-}\sigma$  level and the outer axes label the  $\sigma$ -level. The lower right panel shows the ratio if one explicitly sets all third order moments involving  $v_{\perp}$  to zero (i.e.  $\alpha_{120} = \gamma_{220} = \gamma_{320} = \langle v_{\perp}^2 \delta' \rangle = 0$ ). The effect of  $f_{nl}$  in the mass weighted linear pairwise PDF has the same trend as the uniform weighted PDF: the effect of  $f_{nl}$  is degenerated in the parallel and the perpendicular to the line of separation directions; and the general trend observed in uniform weighted linear PDF still applies – for  $f_{nl} > 0$  the probability of finding infalling pairs increases while the probability of finding pairs moving apart decreases. The inclusion of the mass weighted quantities  $\gamma_{ijk}$  strengthens the effect of  $f_{nl}$  and it is most significant in the decrement in probability of outgoing pairs.

### 3 EVOLVED VELOCITY PDF

Given the linear velocity PDF we now describe a model for the evolution of the PDF. We adopt the Zeldovich Approximation which assumes the comoving velocity remains unchanged. At some initial redshift  $z_i$ , if two particles separated by  $r_i$  have a relative velocity  $(v_{||}^i, v_{\perp a}^i, v_{\perp b}^i)$ . Then at a later redshift  $z = z_0 (\ll z_i)$  the distances traveled are  $D_0/\dot{D}_i(v_{||}^i, v_{\perp a}^i, v_{\perp b}^i)$  (note

that it assumes  $D_0 \gg D_i$ ). Hence the separation of the two particles becomes

$$r^2 = \left( r_i + \frac{D_0}{D_i} v_{\parallel}^i \right)^2 + \left( \frac{D_0}{D_i} \right)^2 (v_{\perp a}^i{}^2 + v_{\perp b}^i{}^2). \quad (24)$$

The evolved relative velocities (with respect to the updated position) are:

$$v_{\parallel} = \frac{\dot{D}_0}{r} \left( \frac{r_i v_{\parallel}^i}{D_i} + \frac{D_0}{D_i^2} v_i^2 \right) \quad (25)$$

$$|v_{\perp}|^2 = v_{\perp a}^2 + v_{\perp b}^2 = \left( \frac{\dot{D}_0}{D_i} v^i \right)^2 - v_{\parallel}^2, \quad (26)$$

where  $v^i{}^2 = v_{\parallel}^i{}^2 + v_{\perp a}^i{}^2 + v_{\perp b}^i{}^2$ . The evolved velocity difference PDF is therefore

$$p(V_{\parallel}, V_{\perp}; R) = \int dr_i dv_{\parallel}^i dv_{\perp a}^i dv_{\perp b}^i \frac{r_i^2}{R^2} p(v_{\parallel}^i, v_{\perp a}^i, v_{\perp b}^i; r) \delta_{\text{D}}(r - R) \delta_{\text{D}}(v_{\parallel} - V_{\parallel}) \delta_{\text{D}}(v_{\perp} - V_{\perp}), \quad (27)$$

(see, for example, Seto & Yokoyama 1998) where the dirac-delta functions use equations (24), (25), and (26) to map the initial quantities to the evolved one. In the following we apply the above formula to compute the evolved velocity difference PDF from equations (6) and (13) and compare the results to measurements from  $N$ -body simulations. We set  $z_i$  and  $z_0$  to be 1100 and 0.5 respectively, justifying the approximation  $D_0 \gg D_i$ .

### 3.1 Comparisons to $N$ -body measurements

We measured the pairwise velocity PDF from a set of  $N$ -body simulations described in Nishimichi et al. (2009). The simulation adopts the *WMAP* 5-years  $\Lambda$ CDM best fit parameters  $(\Omega_m, \Omega_{\Lambda}, \Omega_b, h, \sigma_8, n_s) = (0.279, 0.721, 0.046, 0.701, 0.817, 0.96)$ . The simulation was performed in a box of  $2000 h^{-1}$  Mpc on a side, containing  $512^3$  particles whose mass is  $4.6 \times 10^{12} h^{-1} M_{\odot}$ . The measurements were made from the simulation output at  $z = 0.5$ . To account for the discrete nature of  $N$ -body measurements, separation  $r$  in the following refers to two particles having a separation between  $(r - 2, r + 2)$  in the unit of  $h^{-1}$  Mpc. For the theoretical model we apply the same separation selection in the dirac-delta function of  $r$ . The comparisons of the velocity PDF of  $v_{\parallel}$  and  $v_{\perp}$  are presented in the next two subsections. We will then discuss the implications of the comparisons in the next section.

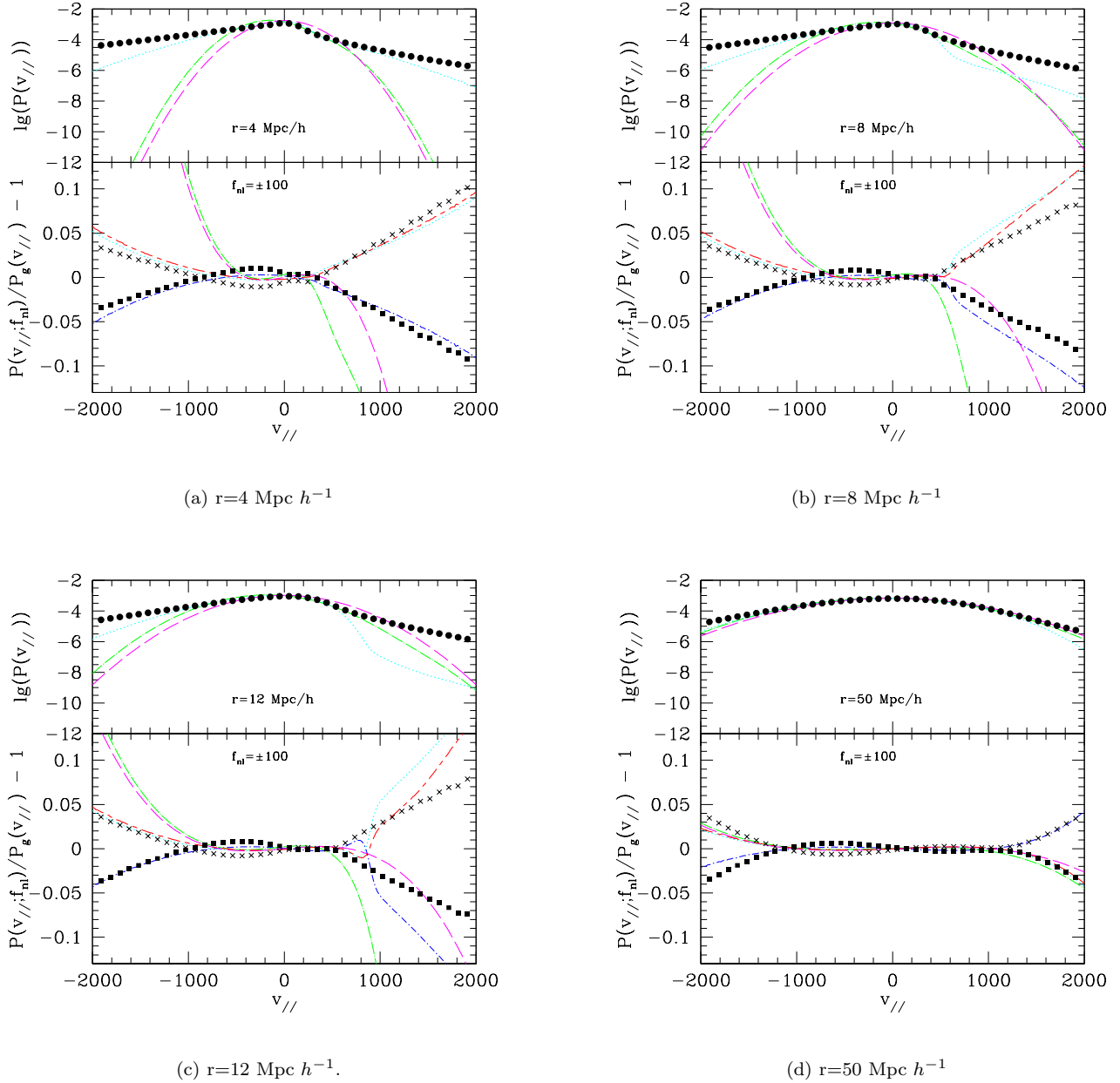
#### 3.1.1 Parallel to the line of separation: $p(v_{\parallel}; r, f_{nl})$

Figure 4 shows the PDF comparisons of the various analytical predictions to the  $N$ -body measurements for the relative velocity parallel to the line of separation for 4 different separations (4, 8, 12, 50  $h^{-1}$  Mpc). The upper panel in each subfigure shows the PDF profile for  $f_{nl} = 0$ : solid symbols are the  $N$ -body measurements, cyan dotted curves are the analytical predictions of equation (27) (marginalized over  $v_{\perp}$ ), green dot-long dashed (mass weighted) and magenta long dashed (uniform weighted) curves are the linear theory predictions respectively.

The predictions from our analytical evolution model give good matches to the  $N$ -body measurements at all scales we investigated, except at large outgoing velocities (i.e.  $v_{\parallel} \gg 0$ ). The agreements with the  $N$ -body measurements are better in small separations (4 and 8  $h^{-1}$  Mpc) than large separation (12  $h^{-1}$  Mpc). The analytical predictions of our model are able to describe the high infalling velocity regimes ( $v_{\parallel} < -1000$ ). This is very encouraging since one may expect that high velocity regions are not described by our simple model. The analytical model also predicts knee-shape transitions at around 300, 600, and 900 km/s for  $r = 4, 8, 12 h^{-1}$  Mpc respectively. Similar but less significant knee-shape changes can be seen from the  $N$ -body measurements around the corresponding velocities. In the high outgoing velocity regions the match is not as good as the infalling regimes. We believe the disagreement in the outgoing velocity regime as compared to the infalling regime is due to non-linear evolution of velocity that is not described by our current model – originally infalling pairs eventually become outgoing (see equation (25)) and non-linear interactions between particles in close contact are not described by the Zeldovich Approximation.

On the other hand, the linear theory predictions do not fare as well as the analytical model's. At small separations the predictions of the linear velocity difference PDF do not match the  $N$ -body measurements – the magenta curves miss both the extrema and the peaks of the PDF at separation  $r = 4, 8, \text{ and } 12 h^{-1}$  Mpc. This is consistent with previous studies that the linear theory uniform weighted velocity PDF does not agree with the velocity correlation in the parallel to the line of separation direction. On the contrary the mass weighted linear predictions provide reasonable matches to the  $N$ -body measurements near the peaks of the PDF at different separations. It confirms the finding of Sheth & Zehavi (2009): the velocity correlation can be described by the linear theory when the mass weighting is taken into account. The matching of the peaks of the PDF guarantees the velocity correlations, which is equivalent to the expected value of the pairwise velocity PDF, would roughly agree. However the mass weighted linear predictions does not match the  $N$ -body measurements when  $|v_{\parallel}|$  is of the order of





**Figure 4.** Pairwise velocity (parallel to line of separation) PDF at different separations. Negative velocity corresponds to particles infalling while positive velocity indicates particles moving away from each other. Upper panels show the pairwise velocity PDF when  $f_{nl} = 0$ : solid symbols are measurements from the  $N$ -body simulation, cyan dotted curves are the velocity difference PDF from the evolution model based on the Zeldovich approximation (equation (27)), green dot-long dashed curves are the linear pairwise velocity ( $q_0$  in equation (17)), and magenta long dashed curves are the linear velocity difference PDF (equation (6)). Lower panels show the ratios of the PDF for  $f_{nl} \pm 100$  to the associated PDF for  $f_{nl} = 0$ : crosses ( $f_{nl} = 100$ ) and solid squares ( $f_{nl} = -100$ ), cyan dotted curves ( $f_{nl} = 100$ ) and blue dot-short dashed curves ( $f_{nl} = -100$ ) are predictions of equation (27), green dot-long dashed curves are the ratios for the linear pairwise PDF ( $f_{nl} = 100$ ), and magenta long dashed curves are the ratios for the linear velocity difference PDF ( $f_{nl} = 100$ ). Red short-long-dashed curves show the prediction from equation (27), neglecting third order moments involving velocity perpendicular to line of separation (see the lower right panel of figure 2).

a few hundreds km/s. The disagreement is getting worse as the separation decreases. At large separation ( $50 h^{-1}\text{Mpc}$ ), the two linear theory predictions are very similar and they describe the  $N$ -body measurements well. They are very close to the prediction of the analytical model and the match to the measurements is only slightly worse at high velocity regimes.

The lower panels of figure 4 show the ratios (subtracted by unity) of the pairwise velocity PDFs for  $f_{nl} = \pm 100$  to the associated PDFs for  $f_{nl} = 0$  at different separations. Measurements from the  $N$ -body simulations are represented by crosses ( $f_{nl} = 100$ ) and squares ( $f_{nl} = -100$ ). Other curves in the lower panels show the PDF ratios of different analytical predictions:

cyan dotted ( $f_{nl} = 100$ ) and blue dot-short dashed ( $f_{nl} = -100$ ) curves are the predictions of the evolution model based on the Zeldovich Approximation (equation (27)); red short-long-dashed curves show the similar predictions for  $f_{nl} = 100$  but setting  $\langle v_{\parallel} v_{\perp}^2 \rangle = 0$  (see the lower right panel of figure 2 for the corresponding linear theory comparison at  $r = 8 h^{-1}\text{Mpc}$ ). The other two curves are the linear theory predicted ratios for  $f_{nl} = 100$ : the magenta long dashed curves are the uniform weighted velocity predictions and the green dot-long dashed curves are the mass weighted velocity predicted ratios.

For the range of separations we investigated the change in the pairwise velocity PDF due to  $f_{nl} = \pm 100$  is at most 5% in the infalling velocity regime and 10% in the outgoing velocity regime. In contrary to the linear theory predictions (see figures 2 and 3, and the magenta long dashed as well as the green dot-long dashed curves), the effect of positive  $f_{nl}$  enhances the probability of having pairs in *both* the infalling and the outgoing high velocity ends. This is true for all the separations we look at, from 4 to 50  $h^{-1}\text{Mpc}$  – scales in which the linear theory is believed to be valid. We also check using a simulation with a smaller box (1  $h^{-1}\text{Gpc}$  on a side) to estimate the box size effect: shrinking the box volume to one-eighth of its size changes the PDF ratios by at most 2% at  $v_{\parallel} = 2000 \text{ km/s}$ .

The predictions of our evolution model, regardless of whether one explicitly set  $\langle v_{\parallel} v_{\perp}^2 \rangle = 0$ , match the  $N$ -body measurements reasonably well when  $r = 4 h^{-1}\text{Mpc}$ . The predicted ratios from the analytic model match the measurements within 2% across the velocity range we look at. It is remarkable to have such agreement at velocity as high as  $\sim 2000\text{km/s}$ . The predicted ratios also match the transition of the PDF from the infalling to the outgoing regime: for  $f_{nl} = 100$  it gradually decreases from positive to negative, then changes direction and become positive again. The same transition is also observed at larger separations and the model’s predictions are able to match the  $N$ -body measurements. In contrast the ratios of the linear theory predictions (both the uniform and the mass weighted) fail to match the  $N$ -body measurements in both infalling and outgoing velocity regimes. While the linear theory predicted ratios still have the same trend as the  $N$ -body measurements in the infalling velocity regime (but the differences between the predictions and the measurements are large), the predicted ratios from linear theory are opposite to the measurements in the outgoing velocity regime (the same is also observed at larger separations). Hence the linear theory cannot be used to predict the effect of  $f_{nl}$  on the pairwise velocity PDF.

At larger separations the agreements in the ratios of the PDF between our analytical model predictions and the  $N$ -body measurements are less impressive: while the predicted ratios still agree well with the measurements in the infalling velocity regime, the differences in the outgoing velocity regime are getting bigger as the separation increases. Nonetheless the predictions still qualitatively match the measurements at  $r = 8$  and  $12 h^{-1}\text{Mpc}$ . At  $r = 50 h^{-1}\text{Mpc}$ , on the other hand, the analytical predictions converge to the linear theory predictions and show opposite trends to the measurements. In the outgoing velocity region, there are some interesting transitions in the analytical model predictions: at  $r = 12 h^{-1}\text{Mpc}$  and  $f_{nl} = 100$ , the predicted ratios (the cyan as well as red curves) first show a decrement at small  $v_{\parallel}$ . They then turn around near  $v_{\parallel} = 800\text{km/s}$  and keep increasing for larger  $v_{\parallel}$ . Such transitions are not seen in the  $N$ -body measurements.

We will leave the discussion on the implications for the discrepancies between the linear theory predictions and the  $N$ -body measurements at all separations as well as the mismatch in the PDF ratios between our analytical models and the measurements at large separations in the next section.

### 3.1.2 Perpendicular to the line of separation: $p(v_{\perp}; r, f_{nl})$

Figure 5 shows the comparisons of the PDFs of the pairwise velocity perpendicular to the line of separation for different separations. The upper panels show the PDF at  $z = 0.5$  for  $f_{nl} = 0$  and the lower panels show the ratios of the PDF for  $f_{nl} = \pm 100$  to the associated PDF for  $f_{nl} = 0$ . The symbol and curve labelings are the same as in figure 4, but we do not show the PDF ratio predictions of the linear theory in the lower panels since the linear theory predicts no effect of  $f_{nl}$  in the marginalized PDF, that is  $p(v_{\perp}; r, f_{nl})/p(v_{\perp}; r, f_{nl} = 0) = 1$ .

The predictions of the PDF profile from our analytical model (equation (27)) match the  $N$ -body measurements reasonably well, except around  $v_{\perp} = 0$  at  $r = 50 h^{-1}\text{Mpc}$ . The predictions agree with the measurements in a wide range of velocity (200 – 1500km/s), as well as the dips near  $v_{\perp} = 0$ . At higher  $v_{\perp}$  the model predictions always underestimate the PDF. The linear theory predictions, on the other hand, fail to match the measured PDF for  $r = 4, 8, \text{ and } 12 h^{-1}\text{Mpc}$ . At  $r = 50 h^{-1}\text{Mpc}$  the linear theory prediction agrees with the  $N$ -body measurements for  $v_{\perp} = 300 - 1200\text{km/s}$ , but it fails to predict the dip near  $v_{\perp} = 0$ . Note that there is no difference between the mass weighted and the uniform weighted linear theory predictions since the correction term due to mass weighting does not depend on  $v_{\perp}$  (equation (17)).

The effect of primordial non-Gaussianity in the pairwise velocity PDF in the perpendicular to the line of separation direction is not as strong as the signature in the parallel to the line of separation direction: the change in the PDF is top at 7% at  $v_{\perp} = 2000\text{km/s}$ . The ratio first shows a decrement (increment) at small  $v_{\perp}$  for  $f_{nl} = 100$  ( $-100$ ). It then gradually switches direction and at high  $v_{\perp}$  show an increment (decrement). This gradual switch from decrement to increment is most significant at small separation. Our analytical model is able to predict the change in the PDF due to primordial non-Gaussianity qualitatively. Its prediction matches the gradual change of the PDF ratios (from decrement to enhancement for  $f_{nl} = 100$ , opposite for  $f_{nl} = -100$ ) and provides a rough approximation on the velocity where the crossing across unity occurs. However the predictions always underestimate the PDF ratios in low  $v_{\perp}$  regime. At higher  $v_{\perp}$  the model prediction on

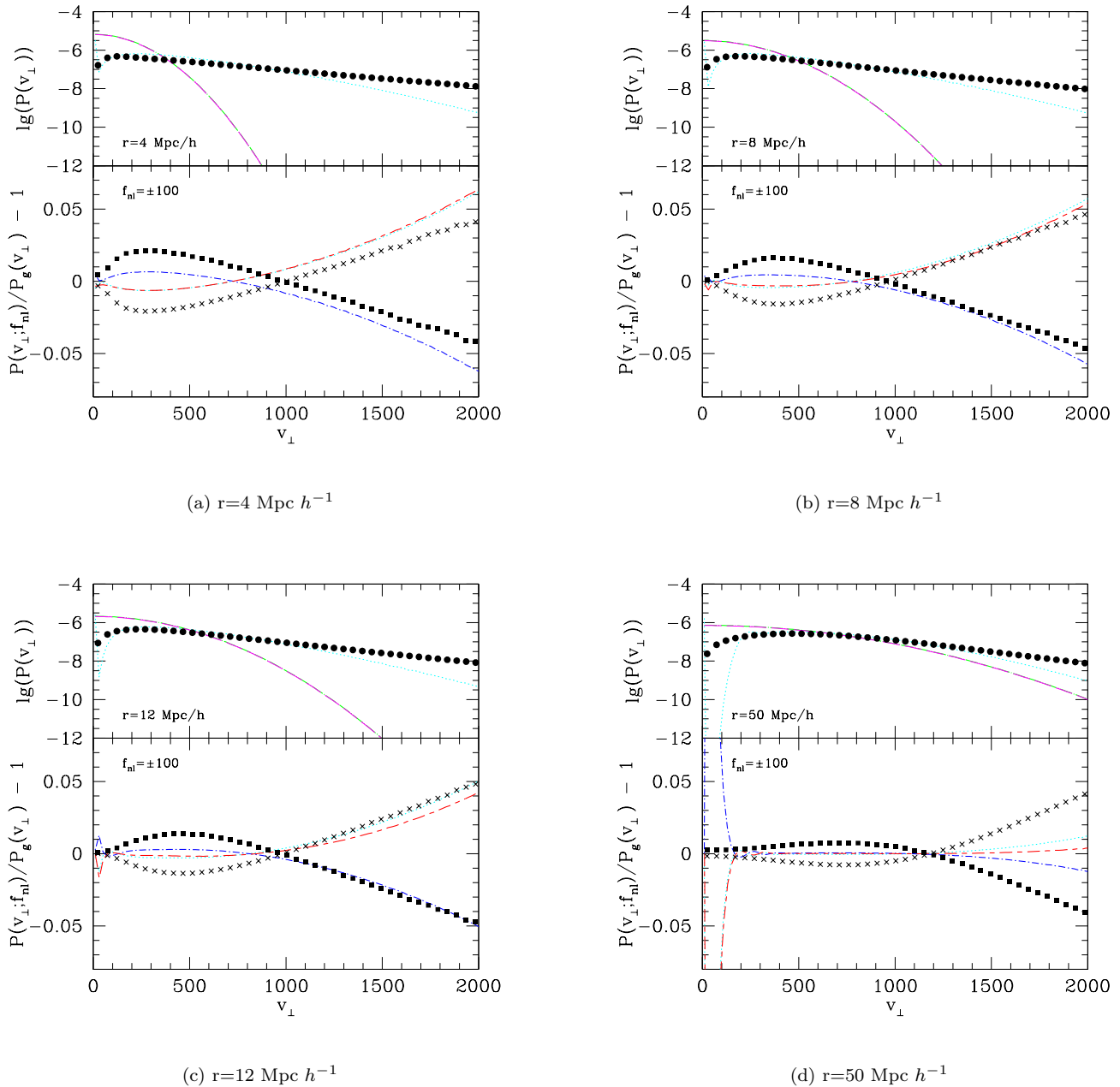


**Figure 5.** Pairwise velocity (perpendicular to line of separation) PDF at different separations. Upper panels show the PDF profile when  $f_{nl} = 0$ : solid symbols are measurements from the  $N$ -body simulation, cyan dotted curves are the prediction from the evolution model based on the Zeldovich Approximation (equation (27)), green dot-long dashed curves are the linear pairwise velocity ( $q_0$  in equation (17)), and magenta long dashed curves are the linear velocity difference PDF (equation (6)). Lower panels show the ratios of the PDF when  $f_{nl} \pm 100$  to the associated PDF for  $f_{nl} = 0$ : crosses ( $f_{nl} = 100$ ) and solid squares ( $f_{nl} = -100$ ) are measurements from  $N$ -body simulation, cyan dotted curves ( $f_{nl} = 100$ ) and blue dot-short dashed curves ( $f_{nl} = -100$ ) are predictions of equation (27). Red short-long-dashed curves show the prediction from equation (27), neglecting third order moments involving velocity perpendicular to line of separation (see the lower right panel of figure 2)

the PDF ratio matches the  $N$ -body measurements very well at  $r = 8$  as well as  $12 h^{-1} \text{Mpc}$ ; the predicted ratio overestimates the change at  $r = 4 h^{-1} \text{Mpc}$  but underestimates at  $r = 50 h^{-1} \text{Mpc}$ . The analytical model predicts the effect of  $f_{nl}$  becomes weaker at some fixed  $v_{\perp}$  for larger  $r$ , the measurements from the  $N$ -body simulations, on the contrary, remain roughly the same at various separations. The measured PDF ratios at high  $v_{\perp}$  only depends on the scale of separation very weakly. In addition there are spikes near  $v_{\perp} = 0$  in the theoretical predicted ratios for  $r = 12$  and  $50 h^{-1} \text{Mpc}$ , but these are not seen in the  $N$ -body simulations.

The linear theory predictions fail to match the  $N$ -body measurements at all separations – it predicts no change in the

pairwise velocity PDF in the perpendicular to the line of separation direction. The  $N$ -body measurements, on the other hand, has several percent-level change in the PDF throughout the velocity range we look at.

#### 4 DISCUSSIONS

We have studied how primordial non-Gaussianity affects the probability density function of the pairwise velocity. Our study complements earlier studies on the signatures of primordial non-Gaussianity on other large-scale structure probes which utilize the modification in the density field (for example the PDF of density field, halo/void abundances, scale dependent halo bias). We have shown that primordial non-Gaussianity models with a non-vanishing bispectrum result in two non-vanishing third-order connected moments of the peculiar velocity ( $\langle v_{\parallel}^3 \rangle$  and  $\langle v_{\parallel} v_{\perp}^2 \rangle$ ). We adopt the local  $f_{nl}$  type primordial non-Gaussianity as an example to compute the modification in the linear velocity difference PDF. Following suggestions by earlier studies, we investigate the effect of  $f_{nl}$  on the linear pairwise velocity PDF. Primordial non-Gaussianity induces correlations between velocities in the parallel and the perpendicular to the line of separation directions. Hence both the uniform weighted and the mass weighted linear velocity PDF can no longer be written as a product of the corresponding univariate PDFs. Furthermore the change in the linear velocity PDF is degenerated in the  $(v_{\parallel}, v_{\perp})$  plane.

Next we have developed an analytical model to describe the evolution of the velocity PDF. It employs the Zeldovich Approximation which assumes the comoving velocity remains unchanged. We then compared the pairwise velocity PDF measured from a  $N$ -body simulation with the predictions from our analytical model at various separations, ranging from 4 to 50  $h^{-1}$ Mpc. Our model predictions agree well with the PDF profiles measured from the  $N$ -body simulation at various separations when  $f_{nl} = 0$  in both the parallel and in the perpendicular to the line of separation directions.

Linear theory fails in matching the  $N$ -body measurements: both the linear velocity difference PDF as well as the linear pairwise velocity PDF fail to predict the PDF profiles and the change in the PDF due to a non-zero  $f_{nl}$ . The linear theory prediction does not take into account the movement of particles: pairs separated by  $r$  having a relative velocity  $(v_{\parallel}, v_{\perp a}, v_{\perp b})$  must have had different separations at earlier redshift. The relative velocities at earlier redshifts also change in general due to the difference in the particles' positions. In other words linear theory is a good approximation only when the displacement of the particles is small compared to the separation between them. For example the displacement associated with a relative velocity  $v = 1000$  km/s is approximately 10  $h^{-1}$ Mpc at  $z = 0.5$  if the velocity remains unchanged. Therefore, only for large enough separations ( $r \gg 10h^{-1}$ Mpc) the linear theory can approximate the PDF. The initial separation and the initial relative velocity determine the evolved separation and the pairwise velocity – equations (24) to (26) give an example of such an evolution model using the Zeldovich approximation. In general the mapping from the initial parameters  $\{r^i, v_{\parallel}^i, v_{\perp}^i\}$  to the evolved parameters  $\{r, v_{\parallel}, v_{\perp}\}$  is non-linear and more than one set of  $\{r^i, v_{\parallel}^i, v_{\perp}^i\}$  would evolve to  $\{r, v_{\parallel}, v_{\perp}\}$ . This analytical model provides results that match the measurements much better than the linear theory.

Including evolution is also important in explaining the change in the PDF due to  $f_{nl}$ . The ratios of the pairwise velocity PDF in the parallel to the line of separation direction can be used to reveal the distribution of pairs with different  $\{r^i, v_{\parallel}^i, v_{\perp}^i\}$  having evolved to the same  $\{r, v_{\parallel}, v_{\perp}\}$ . Recall that the linear theory predicts enhancement in the probability occurs in high velocity infalling pairs and low velocity outgoing pairs when  $f_{nl} > 0$ . On the other hand, the  $N$ -body measurements always have increment in the probability for outgoing pairs. The analytical model provides an algorithm to explain this discrepancy: pairs initially infalling becomes outgoing when they cross each other on the projection on the line of separation. As a result outgoing pairs would be either originally infalling or outgoing pairs. The converse is not true because infalling pairs can only come from pairs that approach each other at earlier redshift. The originally low velocity outgoing pairs, having a higher probability for  $f_{nl} = 100$ , by itself cannot explain the observation from  $N$ -body measurements as the change in the velocity difference PDF associated with these pairs is relative small (recall that the change in the PDF goes as  $v_{\parallel}^3 - 3v_{\parallel}$  and  $v_{\perp}^2 - 1$ ) and cannot account for the level of change in the PDF measured in the simulations. As a result the PDF ratio in the outgoing velocity regime has to be dominated by original infalling pairs.

Our analytical model provides an approximation for the evolution of the velocity difference PDF and it successfully predicts the modification in the velocity PDF due to  $f_{nl}$  qualitatively. The Zeldovich Approximation, on which the analytical model based, does not take into account several important features – it assumes the comoving velocity remains unchanged. This is a good approximation when the separation of the pair in consideration is big. This assumption may not hold when the pair crosses on the projection along the line of separation. Non-linear model is required to describe the evolution of the relative velocity in this cases. As a result the velocity PDF in the regime where cross-over dominates may not be well described by our analytical model.

Another area our analytical model does not describe is the virial motion of particles residing inside dark matter halos. While it is not expected to have pairs residing within the same dark matter halo for the separation we considered in this study, virial motions would certainly affect the distribution of the pairwise velocity.

Notice that our analytical model only describes the evolution of the velocity difference PDF – it is the evolved uniform weighted velocity PDF. In practice it is not what we measured from the  $N$ -body simulation – it is a (evolved) pair weighted

velocity PDF. The comparisons with  $N$ -body measurements show that the evolved velocity difference PDF matches the measurements better than the linear pairwise velocity PDF. Modeling of the non-linear pairwise velocity PDF requires the correlation between the non-linear density contrast and the evolved velocity field. These are not described in the our model and will be left for future study.

It is quite unexpected that the agreement of the analytical model with the  $N$ -body measurement is better at small separation than at large separation. One speculation for that is the simulation measurement is affected by the finite box size effect for big  $r$  – we did check the effect of finite box size by measuring the pairwise velocity PDF from a simulation ran in a box with  $1 h^{-1}\text{Gpc}$  on a side. The resulting PDF at  $r = 50 h^{-1}\text{Mpc}$  agrees qualitatively with the corresponding PDF in the main text. Hence we believe the disagreement in the PDF ratio at  $r = 50 h^{-1}\text{Mpc}$  is not due to the effect of finite box size. Another possibility is the discrepancy is due to the non-linear interactions – here we give two approaches to explain qualitatively how the non-linear interactions affect the velocity PDF. Both are related to the formation of non-linear structures and is not described by the Zeldovich Approximation.

The Zeldovich Approximation assumes the comoving velocity is constant throughout the evolution and it is not a good approximation when non-linear structures (pancake, filament, and halos) form. If the Zeldovich Approximation were the correct model that completely described the evolution, the positive velocity in the evolved velocity difference PDF would be dominated by originally infalling pairs only when  $v_{\parallel} \gtrsim v_0$ , where  $v_0$  corresponds to the velocity that has a displacement approximately equal to the separation  $r$ . This scale also associates with the knee-shape transition in the PDF profiles in the upper panels of figure 4. For  $v_{\parallel} < v_0$  the Zeldovich Approximation predicts originally outgoing pairs should dominate the PDF. Measurements from  $N$ -body simulation, on the other hand, show no such transition. The knee-shape transition in the PDF profiles (upper panels) is also much weaker compared to the analytical predictions. Non-linear evolution models, such as the adhesion model, may be able to explain the difference between the measured and the predicted PDF – while the Zeldovich approximation predicts the velocity PDF is dominated by originally infalling pairs only when  $v_{\parallel} > v_0$ , the frictional dragging term in the adhesion model would damp the velocity, making  $v_0 < v'_{\parallel} \rightarrow v_{\parallel} < v_0$ . As a result the velocity PDF would be dominated by originally infalling pairs at a smaller  $v_{\parallel}$  compared to the Zeldovich Approximation prediction. Notice that this effect will be most significant for big  $r$  as the dragging term is proportional to  $v$ .

The halo model provides another explanation for this discrepancy: in the halo model all particles are residing in halos, each of them acquires its peculiar velocity from two contributions – the virial motion inside the parent halo as well as the bulk movement of the parent halo (Cooray & Sheth 2002; Sheth & Diaferio 2001; Sheth et al. 2001). Hence the relative velocity between pairs residing in different halos (this corresponds to the separations we studied in the current study) can be separated into two parts: the randomly-oriented velocity difference due to the corresponding virial motion and the relative velocity of the two parent halos. The dispersion of the virial motion depends on the mass of the parent halo: more massive halos have a larger dispersion; the bulk velocity of the parent halo depends only weakly on mass. The bulk velocity can be approximated by the linear theory (Cooray & Sheth 2002). At relatively small separations, the two contributions are comparable; at big separations, on the other hand, the two-point correlation function is weak and the velocity is dominated by the virial motion term. It is a well-known fact that there are more massive halos for models with  $f_{nl} > 0$  (see, for example, Lam et al. 2009), hence the velocity dispersion is bigger when  $f_{nl} > 0$ . This effect is most significant in the pairwise velocity PDF for big  $r$  since at such separation the dominant velocity difference is the random-oriented virial velocity difference. The net result is having a higher probability when  $|v_{\parallel}|$  is big but lower probability when  $|v_{\parallel}|$  is small. Our current analytic model does not include the virial motion and as a result it is not able to describe the change in the velocity PDF for large  $r$ . Note that this picture naturally predicts the discrepancy should first show in the outgoing velocity regime – clustered halos attract each other and hence the relative bulk velocity is always infalling when projected on the line of separation of the pairs in consideration. Figure 6 shows the change in the PDF of peculiar velocity for models with  $f_{nl} \neq 0$ . The increase in velocity dispersion and the change in PDF at high  $v$  when  $f_{nl} = 100$  supports this halo model picture in explaining the discrepancy at large separation due to the increase in the magnitude of the virial motion in  $f_{nl}(> 0)$  models.

It is out of the scope of the current study to include these non-linear effect – this will be left for future study. Our current analytic model is able to predict the modification in the pairwise velocity PDF within a few percent level at quasi-linear regime (from  $4 - 12 h^{-1}\text{Mpc}$ ).

While this study focuses on the pairwise velocity of PDF of dark matter, we are in the process to extend the current work to study the effect of primordial non-Gaussianity on the pairwise velocity of biased tracers. We are also extending our study to examine the effect of primordial non-Gaussianity on the redshift space distortion. The  $N$ -body measurements of the pairwise velocity PDF show clearly both the parallel and the perpendicular to the line of separation directions have primordial non-Gaussianity imprints. The effect can be seen in separation as large as  $r = 50 h^{-1}\text{Mpc}$ . Our analytical model improves earlier work (Lam et al. 2010; Schmidt 2010) – it includes the change in the pairwise velocity PDF in both the parallel and the perpendicular directions in the analysis as well as the evolution of the pairwise velocity PDF. As a result it provides a much better match to the  $N$ -body measurements compared to the linear theory. This enables our analytical model to improve the estimation of the signature of primordial non-Gaussianity in the redshift space distortion.

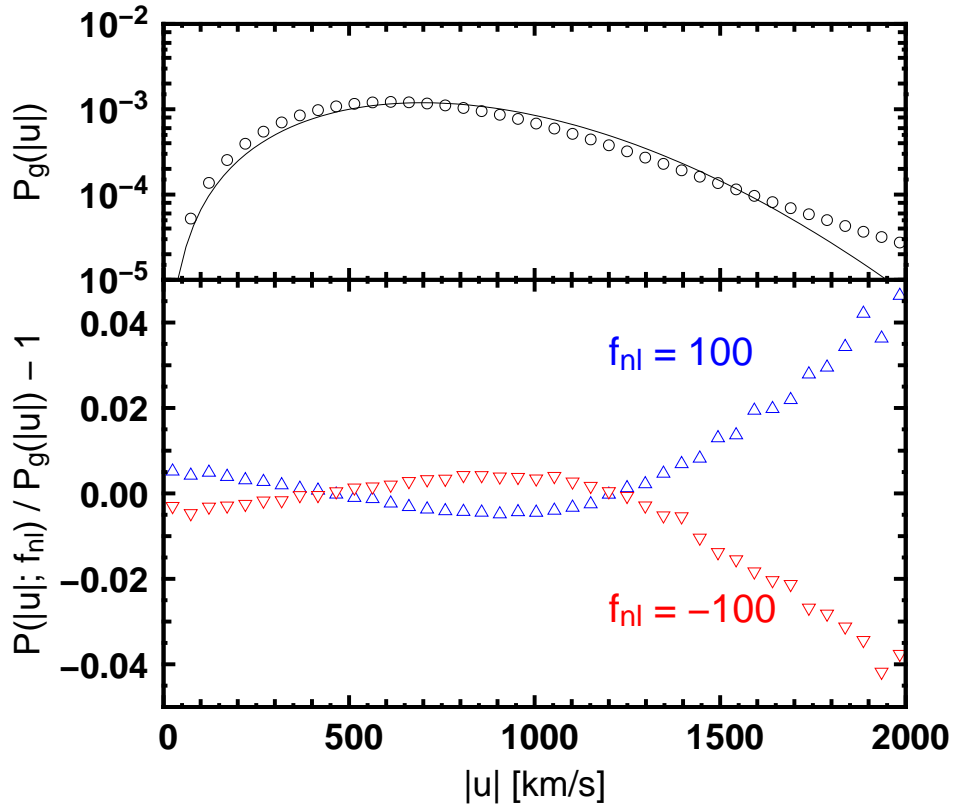


**Figure 6.** The 1-point PDF of peculiar velocity: the upper panel shows the PDF profile of the peculiar velocity when  $f_{nl} = 0$ . The open circles show the measurement from  $N$ -body simulation and the solid curve shows the Maxwellian distribution with  $\sigma$  equal to the velocity dispersion measured from the simulation. The lower panel shows the ratio of the PDF for  $f_{nl} = \pm 100$  to  $f_{nl} = 0$ : upward pointing triangles are the ratio for  $f_{nl} = 100$ ; downward pointing for  $f_{nl} = -100$ . Particles with large velocities ( $> 1000$ km/s) are mostly populated in massive halos.

## ACKNOWLEDGEMENTS

TYL would like to thank Ravi Sheth, Robert Smith, and Vincent Desjacques for the discussion on peculiar velocity field. This work was supported by World Premier International Research Center Initiative (WPI Initiative), MEXT, Japan. TYL is also supported by a kakenhi grant (Grant-in-Aid for Young Scientists (B) – 22740149). T. N. is supported by a Grant-in-Aid for Japan Society for the Promotion of Science (JSPS) Fellows.

## REFERENCES

- Afshordi N., Tolley A. J., 2008, *Phys. Rev. D*, 78, 123507  
 Bernardeau F., Colombi S., Gaztañaga E., Scoccimarro R., 2002, *Phys. Rep.*, 367, 1  
 Bhattacharya S., Kosowsky A., 2007, *Astrophys. J. Lett.*, 659, L83  
 Bhattacharya S., Kosowsky A., 2008, *Journal of Cosmology and Astro-Particle Physics*, 8, 30  
 Buchbinder E. I., Khoury J., Ovrut B. A., 2008, *Physical Review Letters*, 100, 171302  
 Carbone C., Verde L., Matarrese S., 2008, *Astrophys. J. Lett.*, 684, L1  
 Catelan P., Scherrer R. J., 1995, *Astrophys. J.*, 445, 1  
 Chongchitnan S., Silk J., 2010, *ArXiv e-prints*, astro-ph/1007.1230  
 Cooray A., Sheth R., 2002, *Phys. Rep.*, 372, 1  
 Croft R., Efstathiou G., 1995, in J. P. Mücke, S. Gottloeber, & V. Müller ed., *Large Scale Structure in the Universe Constraints on the Power Spectrum of Mass Fluctuations from Galaxy Cluster Peculiar Velocities*. pp 101–+  
 Cunha C., Huterer D., Dore O., 2010, *ArXiv e-prints*, astro-ph/1003.2416  
 Dalal N., Doré O., Huterer D., Shirokov A., 2008, *Phys. Rev. D*, 77, 123514  
 Desjacques V., Seljak U., 2010a, *ArXiv e-prints*, astro-ph/1003.5020  
 Desjacques V., Seljak U., 2010b, *Phys. Rev. D*, 81, 023006  
 Desjacques V., Seljak U., Iliev I. T., 2009, *Mon. Not. R. Astron. Soc.*, 396, 85

- Giannantonio T., Porciani C., 2010, *Phys. Rev. D*, 81, 063530
- Gorski K., 1988, *Astrophys. J. Lett.*, 332, L7
- Grossi M., Branchini E., Dolag K., Matarrese S., Moscardini L., 2008, *Mon. Not. R. Astron. Soc.*, 390, 438
- Grossi M., Verde L., Carbone C., Dolag K., Branchini E., Iannuzzi F., Matarrese S., Moscardini L., 2009, ArXiv e-prints, astro-ph/0902.2013
- Hahn T., 2005, *Computer Physics Communications*, 168, 78
- Hamana T., Kayo I., Yoshida N., Suto Y., Jing Y. P., 2003, *Mon. Not. R. Astron. Soc.*, 343, 1312
- Hikage C., Matsubara T., Coles P., Liguori M., Hansen F. K., Matarrese S., 2008, *Mon. Not. R. Astron. Soc.*, 389, 1439
- Izumi K., Soda J., 2007, *Phys. Rev. D*, 76, 083517
- Kamionkowski M., Verde L., Jimenez R., 2009, *Journal of Cosmology and Astro-Particle Physics*, 1, 10
- Khoury J., Piazza F., 2008, ArXiv e-prints, hep-th/0811.3633
- Komatsu E., 2010, ArXiv e-prints, astro-ph/1003.6097
- Komatsu E., Smith K. M., Dunkley J., Bennett C. L., Gold B., Hinshaw G., Jarosik N., Larson D., Nolte M. R., Page L., Spergel D. N., Halpern M., Hill R. S., Kogut A., Limon M., Meyer S. S., Odegard N., Tucker G. S., Weiland J. L., Wollack E., Wright E. L., 2010, ArXiv e-prints, astro-ph/1001.4538
- Koyama K., Soda J., Taruya A., 1999, *Mon. Not. R. Astron. Soc.*, 310, 1111
- Kuwabara T., Taruya A., Suto Y., 2002, *Publ. Astron. Soc. Japan*, 54, 503
- Lam T. Y., Desjacques V., Sheth R. K., 2010, *Mon. Not. R. Astron. Soc.*, 402, 2397
- Lam T. Y., Sheth R. K., 2009, *Mon. Not. R. Astron. Soc.*, 395, 1743
- Lam T. Y., Sheth R. K., Desjacques V., 2009, *Mon. Not. R. Astron. Soc.*, 399, 1482
- Liguori M., Sefusatti E., Fergusson J. R., Shellard E. P. S., 2010, ArXiv e-prints, astro-ph/1001.4707
- Lo Verde M., Miller A., Shandera S., Verde L., 2008, *Journal of Cosmology and Astro-Particle Physics*, 4, 14
- Marian L., Hilbert S., Smith R. E., Schneider P., Desjacques V., 2010, ArXiv e-prints, arXiv:1010.5242
- Matarrese S., Verde L., 2008, *Astrophys. J. Lett.*, 677, L77
- Matarrese S., Verde L., Jimenez R., 2000, *Astrophys. J.*, 541, 10
- McDonald P., 2008, *Phys. Rev. D*, 78, 123519
- McEwen J. D., Hobson M. P., Lasenby A. N., Mortlock D. J., 2008, *Mon. Not. R. Astron. Soc.*, 388, 659
- Nishimichi T., Taruya A., Koyama K., Sabiu C., 2009, ArXiv e-prints, astro-ph/0911.4768
- Peel A. C., 2006, *Mon. Not. R. Astron. Soc.*, 365, 1191
- Pillepich A., Porciani C., Hahn O., 2008, ArXiv e-prints, astro-ph/0811.4176
- Rossi G., Chingangbam P., Park C., 2010, ArXiv e-prints, astro-ph/1003.0272
- Rossi G., Sheth R. K., Park C., Hernandez-Montenegro C., 2009, ArXiv e-prints, astro-ph/0906.2190
- Sartoris B., Borgani S., Fedeli C., Matarrese S., Moscardini L., Rosati P., Weller J., 2010, ArXiv e-prints, astro-ph/1003.0841
- Scherrer R. J., 1992, *Astrophys. J.*, 390, 330
- Schmidt F., 2010, ArXiv e-prints, astro-ph/1005.4063
- Scoccimarro R., 2004, *Phys. Rev. D*, 70, 083007
- Scoccimarro R., Sefusatti E., Zaldarriaga M., 2004, *Phys. Rev. D*, 69, 103513
- Sefusatti E., Komatsu E., 2007, *Phys. Rev. D*, 76, 083004
- Seto N., Yokoyama J., 1998, *Astrophys. J.*, 492, 421
- Sheth R. K., Diaferio A., 2001, *Mon. Not. R. Astron. Soc.*, 322, 901
- Sheth R. K., Diaferio A., Hui L., Scoccimarro R., 2001, *Mon. Not. R. Astron. Soc.*, 326, 463
- Sheth R. K., Hui L., Diaferio A., Scoccimarro R., 2001, *Mon. Not. R. Astron. Soc.*, 325, 1288
- Sheth R. K., Zehavi I., 2009, *Mon. Not. R. Astron. Soc.*, 394, 1459
- Silvestri A., Trodden M., 2008, ArXiv e-prints, astro-ph/0811.2176
- Slosar A., 2009, *Journal of Cosmology and Astro-Particle Physics*, 3, 4
- Slosar A., Hirata C., Seljak U., Ho S., Padmanabhan N., 2008, *Journal of Cosmology and Astro-Particle Physics*, 8, 31
- Smidt J., Amblard A., Byrnes C. T., Cooray A., Munshi D., 2010, ArXiv e-prints, astro-ph/1004.1409
- Smith R. E., Desjacques V., Marian L., 2010, ArXiv e-prints, arXiv:1009.5085
- Taruya A., Koyama K., Matsubara T., 2008, *Phys. Rev. D*, 78, 123534
- Tselikhovich D., Hirata C., Slosar A., 2010, ArXiv e-prints
- Wands D., 2010, ArXiv e-prints, astro-ph/1004.0818
- Xia J., Viel M., Baccigalupi C., De Zotti G., Matarrese S., Verde L., 2010, ArXiv e-prints, astro-ph/1003.3451
- Yadav A. P. S., Wandelt B. D., 2008, *Physical Review Letters*, 100, 181301
- Yoshida N., Sheth R. K., Diaferio A., 2001, *Mon. Not. R. Astron. Soc.*, 328, 669

**APPENDIX A: DERIVATION OF MASS WEIGHTED LINEAR PAIRWISE VELOCITY PDF**

This appendix derives the expression of the linear pairwise velocity PDF for  $f_{nl} \neq 0$  (equation (20)). The following derivation also applies to the derivations of the linear velocity difference PDF when  $f_{nl} \neq 0$  (equation (13), by setting  $\delta = \delta' = 0$  in the following derivation) and the linear pairwise velocity PDF when  $f_{nl} = 0$  (equation (17)).

The first step is to generalize the expression for the line-of-sight pairwise velocity generating function  $\mathcal{M}$  (equation (8) in Scoccimarro (2004)) to the 3d generating function of pairwise velocity:

$$\mathcal{Z}(\boldsymbol{\lambda}; r) \equiv [1 + \xi(r)]\mathcal{M}(\boldsymbol{\lambda}; r) = \langle \exp(\boldsymbol{\lambda} \cdot \mathbf{v}) [1 + \delta(x)] [1 + \delta(x')] \rangle, \quad (\text{A1})$$

where  $\boldsymbol{\lambda} \cdot \mathbf{v} = \lambda_{\parallel} v_{\parallel} + \lambda_{\perp a} v_{\perp a} + \lambda_{\perp b} v_{\perp b}$  and  $x = x' + r$ . The characteristics function can be computed using the cumulants (see discussion in Scoccimarro (2004)):

$$\begin{aligned} \mathcal{Z}(i\boldsymbol{\lambda}; r) &= \exp(\exp(i\boldsymbol{\lambda} \cdot \mathbf{v}))_c [1 + \langle \exp(i\boldsymbol{\lambda} \cdot \mathbf{v})(\delta + \delta') \rangle_c + \langle \exp(i\boldsymbol{\lambda} \cdot \mathbf{v})\delta \rangle_c \langle \exp(i\boldsymbol{\lambda} \cdot \mathbf{v})\delta' \rangle_c + \langle \exp(i\boldsymbol{\lambda} \cdot \mathbf{v})\delta\delta' \rangle_c] \\ &= \exp \left[ \sum_j \frac{\langle v_j^2 \rangle}{2} (i\lambda_j)^2 + \frac{\langle v_{\parallel}^3 \rangle}{3!} (i\lambda_{\parallel})^3 + \frac{\langle v_{\parallel} v_{\perp a}^2 \rangle}{2} (i\lambda_{\parallel})(i\lambda_{\perp a})^2 + \frac{\langle v_{\parallel} v_{\perp b}^2 \rangle}{2} (i\lambda_{\parallel})(i\lambda_{\perp b})^2 + \dots \right] \\ &\quad \times \left\{ 1 + \xi(r) + \langle v_{\parallel} \delta \delta' \rangle (i\lambda_{\parallel}) + \sum_j \left[ \langle v_j (\delta + \delta') \rangle (i\lambda_j) + \frac{\langle v_j^2 (\delta + \delta') \rangle}{2} (i\lambda_j)^2 + \dots \right] \right. \\ &\quad \left. + \left[ \sum_j \langle v_j \delta \rangle (i\lambda_j) + \frac{\langle v_j^2 \delta \rangle}{2} (i\lambda_j)^2 + \dots \right] \left[ \sum_j \langle v_j \delta' \rangle (i\lambda_j) + \frac{\langle v_j^2 \delta' \rangle}{2} (i\lambda_j)^2 + \dots \right] + \dots \right\}, \end{aligned} \quad (\text{A2})$$

where  $\delta \equiv \delta(x)$ ,  $\delta' \equiv \delta(x')$ , and the summation over  $j$  denotes summing over all three directions  $\{\parallel, \perp a, \perp b\}$ . The first term in the second equity is the linear velocity difference characteristic function while the second term is associated with the mass weighting. The characteristic function for the linear velocity difference for  $f_{nl} = 0$ ,

$$\mathcal{F}_0(i\boldsymbol{\lambda}; r) = \exp \left[ \sum_j \frac{\langle v_j^2 \rangle}{2} (i\lambda_j)^2 \right], \quad (\text{A4})$$

whose Fourier transform is the linear velocity difference PDF when  $f_{nl} = 0$  (equation (6)). Hence we can factorize  $\mathcal{F}_0$  from  $\mathcal{Z}$  and define  $\mathcal{G}$

$$\mathcal{Z}(i\boldsymbol{\lambda}; r) \equiv \mathcal{G}(i\boldsymbol{\lambda}; r) \mathcal{F}_0(i\boldsymbol{\lambda}; r) \quad (\text{A5})$$

So far the expression is exact. Now we take the approximation that only terms up to the first order in  $f_{nl}$  is included and notice that  $\langle v_{\perp a} \delta \rangle = \langle v_{\perp b} \delta \rangle = 0$ . Hence

$$\begin{aligned} \mathcal{G}(i\boldsymbol{\lambda}; r) &= 1 + \xi(r) + (\langle v_{\parallel} \delta \rangle + \langle v_{\parallel} \delta' \rangle + \langle v_{\parallel} \delta \delta' \rangle) (i\lambda_{\parallel}) + \langle v_{\parallel} \delta \rangle \langle v_{\parallel} \delta' \rangle (i\lambda_{\parallel})^2 + \left[ \frac{\langle v_{\parallel}^3 \rangle}{3!} (1 + \xi(r)) + \frac{\langle v_{\parallel} \delta \rangle \langle v_{\parallel}^2 \delta' \rangle}{2} + \frac{\langle v_{\parallel} \delta' \rangle \langle v_{\parallel}^2 \delta \rangle}{2} \right] (i\lambda_{\parallel})^3 \\ &\quad + \frac{\langle v_{\parallel}^3 \rangle}{3!} (\langle v_{\parallel} \delta \rangle + \langle v_{\parallel} \delta' \rangle) (i\lambda_{\parallel})^4 + \frac{\langle v_{\parallel}^3 \rangle}{3!} \langle v_{\parallel} \delta \rangle \langle v_{\parallel} \delta' \rangle (i\lambda_{\parallel})^5 + \sum_{\alpha=a,b} \Gamma(i\lambda_{\perp \alpha}), \end{aligned} \quad (\text{A6})$$

where

$$\begin{aligned} \Gamma(i\lambda_{\perp \alpha}) &= \left[ \frac{\langle v_{\parallel} \delta \rangle \langle v_{\perp \alpha}^2 \delta' \rangle}{2} + \frac{\langle v_{\parallel} \delta' \rangle \langle v_{\perp \alpha}^2 \delta \rangle}{2} + \frac{\langle v_{\parallel} v_{\perp \alpha}^2 \rangle}{2} (1 + \xi(r)) \right] (i\lambda_{\parallel})(i\lambda_{\perp \alpha})^2 + \frac{\langle v_{\parallel} v_{\perp \alpha}^2 \rangle}{2} (\langle v_{\parallel} \delta \rangle + \langle v_{\parallel} \delta' \rangle) (i\lambda_{\parallel})^2 (i\lambda_{\perp \alpha})^2 \\ &\quad + \frac{\langle v_{\parallel} v_{\perp \alpha}^2 \rangle}{2} \langle v_{\parallel} \delta \rangle \langle v_{\parallel} \delta' \rangle (i\lambda_{\parallel})^3 (i\lambda_{\perp \alpha})^2. \end{aligned} \quad (\text{A7})$$

To get the mass weighted linear PDF we need to do a Fourier transform on  $\mathcal{Z}$ . While the expression seems very complicated, the Fourier transform can be done analytically due to the fact that the Fourier transform of  $\mathcal{G}$  is actually a derivative operator acting on the uniform weighted linear PDF. Recall that the uniform weighted linear PDF is a product of three univariate PDFs, hence the derivative operation can be done easily and the resulting mass weighted linear pairwise velocity PDF is equation (20).